Neutrino oscillations at Super-Kamiokande.

Danuta Kiełczewska

Institute for Experimental Physics, Warsaw University,
Hoża 69, Warsaw, Poland
and
Physics Department, University of California,
Irvine, CA 92697

for THE SUPER-KAMIOKANDE COLLABORATION.

Recent results on atmospheric and solar neutrinos collected in the Super-Kamiokande detector are presented. The high precision measurement of angular distribution of atmospheric neutrinos confirms the evidence for neutrino oscillations announced by the Super-Kamiokande in 1998. The deficit of the observed solar neutrino flux compared to the predictions of the standard solar model, often interpreted by neutrino oscillations, is further studied with precise measurement of the neutrino energy spectrum above 5.5 MeV.

1. Introduction

Atmospheric neutrinos are produced by cosmic rays in the Earth's upper atmosphere. As a result of a power-law momentum spectrum of primary cosmic rays the neutrinos have mostly energies of a few GeV. They arise mainly from the decay chain $\pi \to \mu\nu_\mu, \mu \to e\nu_\mu\ \nu_e$ and thus at low energies they are composed of muon and electron flavor at a proportion of 2:1.

Calculations of the absolute flux of atmospheric neutrinos [1,2] suffer from a fairly large uncertainties ($\sim 20\%$) of the measured fluxes of cosmic rays. However the ratio of muon to electron flavor content is calculated with an error of less than 5%. The measurements of this ratio over last decade indicated a deficit of muon neutrinos [3–5] but systematic uncertainties in models of neutrino interactions prevented an unique interpretation of the effect.

The Cherenkov technique allows to determine the direction of the produced charged leptons and hence the pathlengths travelled by neutrinos. They range from about 15 km for neutrinos produced directly overhead, to ~13000 km for neutrinos produced at antipodes. The attenuation of the flux of neutrinos passing the Earth is insignificant and so a study of angular distribution allows for a sensitive test of the neutrino oscillation hypothesis.

An up-down asymmetry was first observed by Kamiokande group [6]. Much larger data sample available in Super-Kamiokande allowed for precision measurements of the shape of the angular distribution free from uncertainties of the lepton flavor ratio and provided the evidence for $\nu_\mu \leftrightarrow \nu_x$ oscillations [7,8].

The probability of flavor conversion in a simple two-flavor mixing scheme and for neutrino propagation in vacuum is

$$P_{i\to f} = \sin^2 2\theta \sin\left(\frac{1.27\Delta m^2(\mathrm{eV}^2)L(\mathrm{km})}{E_\nu(\mathrm{GeV})}\right), \quad (1)$$

where Δm^2 denotes the difference of squares of masses of the states rotated by θ with respect to the weak-interaction states and L is the neutrino pathlength.

It is seen from the formula that solar neutrinos with much larger L/E_ν ratio allow to probe much smaller range of Δm^2. Moreover a resonant enhancement of oscillations (MSW effect [9]) in dense matter of the solar core makes experiments sensitive to much smaller mixing angles.

A significant deficit of electron neutrinos arriving from the Sun has been reported by four different experiments [10]. The Super-Kamiokande offers a possibility to test the oscillation hypoth-

esis in a model-independent way by looking for a distortion of the recoil energy spectrum [11] with respect to the shape expected from the decay

$^8\mathrm{B} \longrightarrow {}^8\mathrm{Be}^* + e^+ + \nu_e.$

Another effect which could reveal new physics of neutrinos is a possible regeneration of ν_e flux in their passage through the Earth core due to MSW effect. Hence differences in observations during day and night are studied [12].

We report here the updated results on both atmospheric (848 day sample) and solar neutrinos (708 day sample).

2. The Super-Kamiokande Detector

The Super-Kamiokande experiment is a large water Cherenkov detector located in Mozumi, Japan. Its total mass of ultra-pure water is 50 kton, divided into two concentric cylinders: an inner volume with its inside surface covered by 11146 inward-looking 50 cm photomultiplier tubes, and an outer volume serving as entering particle shield and veto with 1885 outward-looking 20 cm phototubes. The fiducial mass of the inner volume (2 m away from the walls) is 22.5 kton. The data taking started in April 1996.

3. Atmospheric Neutrinos

A sample of atmospheric neutrinos consists mainly of the interactions occuring inside the fiducial volume of the detector, called *contained* events. They are subdivided into "sub-GeV" (with visible energy <1.33 GeV) and "multi-GeV" (>1.33 GeV) events. The events are called fully contained (FC) if charged products do not leave the inner detector volume, otherwise they are classified as partially contained (PC). According to MC simulations 98% of PC events are ν_μ CC interactions.

The interactions occuring in the rock outside of the detector are also considered if they produce *upward-going muons*, as the downward-going neutrino-induced muons could not be distinguished from much more numerous cosmic ray muons. The upward-going muons can either traverse the entire detector ("through-going") or stop inside it.

The neutrino energies for different classes of events are displaed in Fig. 1

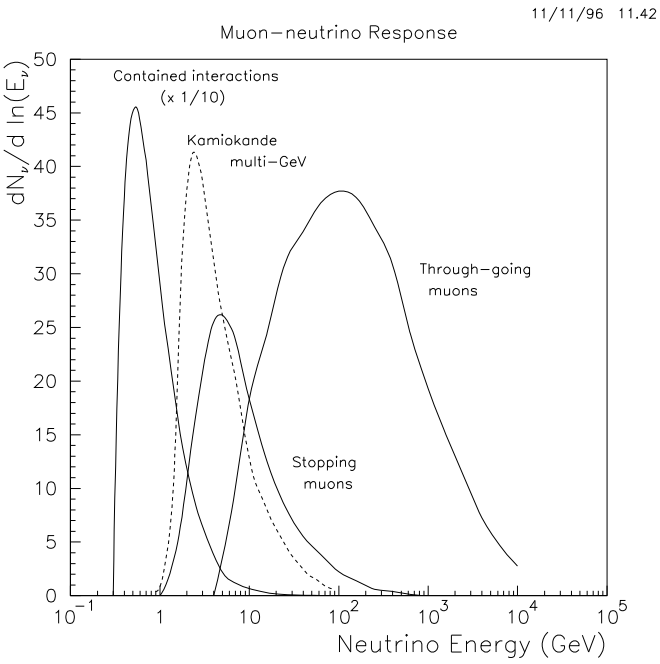

Figure 1. Energy distribution of parent neutrinos that produce event categories described in the text (adapted from T.K. Gaisser preprint [13]).

Details of the event selection and reconstruction are described elsewhere [7,14].

3.1. Contained events

Cherenkov rings can be separated into 2 categories: "e-like" or showering type topology for electromagnetic cascades resulting from electrons and gammas and "μ-like" topology for muons and charged pions. The separation is essentially based on how sharp are the ring edges. Protons are rarely produced above Cherenkov threshold.

In order to tag the neutrino flavor a sample of single ring events is selected, which is dominated by quasi-elastic interaction:

$$\nu_l + N \rightarrow l + N'. \qquad (2)$$

The data are compared with samples of simulated neutrino interactions, with the particles and light emitted by them carefully propagated

Table 1
Contained events collected in 848 days.

	Sub-GeV		Multi-GeV	
	Data	MC	Data	MC
Single ring:				
e-like	1826	1754	439	414
μ-like	1852	2617	351	487
Multiple ring	1456	1871	867	1080
PC (μ-like)			470	656
Total	5134	6242	2127	2637

in the detector. The MC sample is subjected to the same analysis as the data. Hence we estimate that the single ring FC e-like and μ-like samples contain 86% and 96% of CC ν_e and ν_μ interactions respectively.

3.1.1. Event rates

Table 1 displays the numbers of contained events in the 848 day sample.

The measured flavor ratio is conventionally compared to expectation as the "ratio of ratios", R, defined as

$$R = \frac{(N_\mu/N_e)_{DATA}}{(N_\mu/N_e)_{MC}}, \quad (3)$$

where N_μ and N_e are numbers of μ-like and e-like events for data and MC. Using the neutrino fluxes from Ref. [1] one obtains:

$$R_{subGeV} = 0.68 \pm 0.02(\text{stat}) \pm 0.05(\text{sys})$$
$$R_{multiGeV} = 0.68 \pm 0.04(\text{stat}) \pm 0.08(\text{sys})$$

For no oscillations, R is expected to be 1. However, R is significantly smaller than 1 for both sub-GeV and multi-GeV data.

3.1.2. Angular distributions of single ring events

At energies relevant for atmospheric neutrinos there is no flux attenuation in Earth and so an approximate up-down symmetry is expected. However cosmic rays of a few GeV are deflected by the geomagnetic field and this affects neutrino directions. To check the reliability of both our experimental results and the atmospheric neutrino flux calculations, we have selected a sample of nearly horizontal single ring events ($|\cos\theta| < 0.5$, where θ is zenith angle) with momentum between 400 and 3000 MeV/c.

Fig. 2 shows the azimuthal distribution for both e-like and μ-like events, along with two flux predictions[1,16]. The expected deficit from the east is observed. This analysis has been described in detail in Ref. [17].

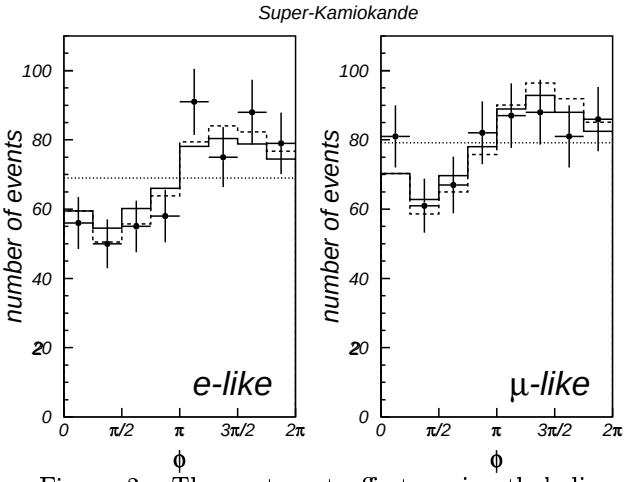

Figure 2. The east-west effect: azimuthal distribution of nearly horizontal e-like and μ-like events, along with MC predictions based on Honda (solid line) and Bartol (dashed line) fluxes. $\phi = 0$ corresponds to particles going to the north and $\phi = \pi$ corresponds to particles going to the south. The expected deficit of neutrinos from the east due to the geomagnetic cutoff of the charged primaries is observed.

The agreement between the data and calculations provides some evidence that geomagnetic effects are correctly accounted for in the flux predictions. We then compare the experimental and theoretical distributions of zenith angle. In what follows $\cos\theta = -1$ corresponds to upward-going neutrinos and $\cos\theta = +1$ corresponds to

downward-going. Angular distributions for different event categories are are compared with MC simulations in Fig. 3. A deficit of muon neutrinos passing through the Earth is clearly seen, while the obsereved angular distribution of e-like events agrees in shape with simulations.

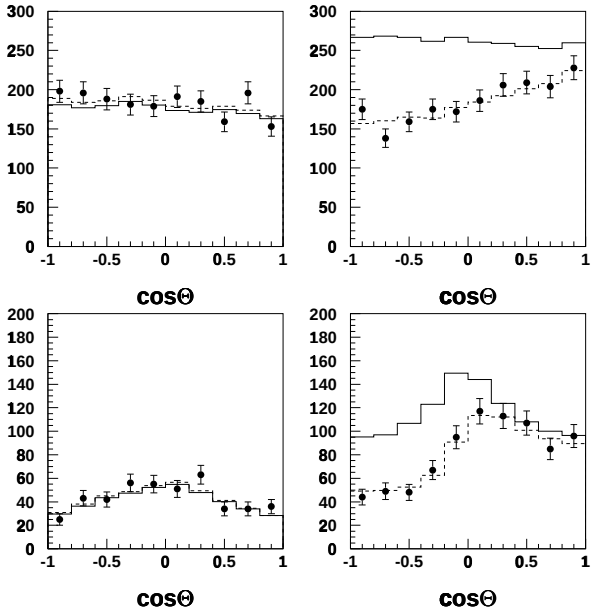

Figure 3. Preliminary angular distributions for sub-GeV (top) and multi-GeV (bottom) 848 day samples; left figures are for e-like and right for μ-like events. Solid lines show the MC no-oscillation prediction, and broken lines show the $\nu_\mu \leftrightarrow \nu_\tau$ oscillation prediction for the best-fit parameters.

In Fig. 4 an up-down asymmetry $A = \frac{U-D}{U+D}$ is shown as a function of momentum for e-like and μ-like events. The up-going U and down-going D particles are defined with $|\cos\theta| > 0.2$

In order to test the oscillation hypotheses the single ring contained data were divided into 70 bins according to the event energies and directions. A χ^2 was constructed to compare the observed event numbers with those resulted from MC simulations assuming different oscillation parameters. Additional terms in the χ^2 take into account systematic uncertainties. The flux nor-

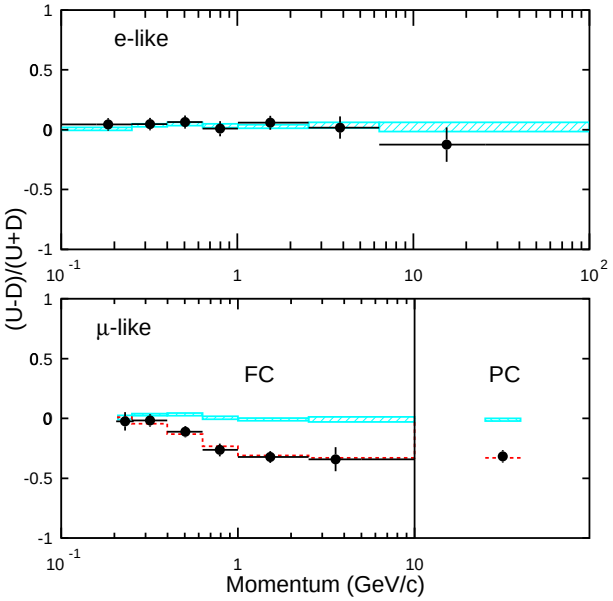

Figure 4. Up-down asymmetry as a function of momentum for e-like and μ-like events. The dashed line shows the $\nu_\mu \leftrightarrow \nu_\tau$ oscillation prediction for the best-fit parameters.

malization is treated as a free parameter. The details of the procedure are described in [8,15].

Assuming $\nu_\mu \leftrightarrow \nu_\tau$ oscillations the best fit for 848 day sample is obtained for $\sin^2 2\theta = 0.995$ and $\Delta m^2 = 3.0 \times 10^{-3}$ eV^2, with $\chi^2/d.o.f. = 55/67$, while for no-oscillation hypothesis it is 177/69, corresponding to a probability of less than 0.0001%. The histograms for the best fit parameters are superimposed in Fig. 3 and 4.

Oscillation of ν_μ to non-interacting "sterile" neutrinos also fit the data well [15]: the best fit for 736 day sample is obtained for $\sin^2 2\theta = 1.0$ and $\Delta m^2 = 4.5 \times 10^{-3}$ eV^2, with $\chi^2/d.o.f. = 64/67$.

On the other hand in the two-flavor mixing scheme considered here the sole $\nu_\mu \leftrightarrow \nu_e$ transformation is excluded with $\chi^2/d.o.f. = 110/67$ ($P < 0.1\%$).

3.1.3. Angular distributions of 2-ring events

Multi ring sample consists of ν interactions with pion production. As particle identification becomes more ambiguous for overlapping rings we first analyze 2-ring events. Cherenkov ring pattern is essentially indistinguishable between muons and charged pions, so special cuts were developed in order to separate the sample into ν_e and ν_μ enriched subsamples. The details of the selection can be found in [14].

According to simulations, the ν_e enriched category is 56% ν_e CC, 12% ν_μ CC and 31% NC, while the ν_μ enriched is 90% ν_μ CC, 2% ν_e CC and 8% NC. The angular distributions for the preliminary analysis of 848 day data are shown in Figure 5. Clearly, the 2-ring sample is consistent with the oscillation hypothesis.

3.2. Upward-going muons

The upward-going muon sample makes it possible to probe higher neutrino energies (c.f. Fig. 1). With an interaction point outside of the detector the event energy cannot be measured. However a relative rate of stopping to through-going samples compared to MC expectations provides an independent information about the energy dependence of oscillations. Moreover at those high energies a muon direction is very well correlated with that of a parent neutrino. Fig. 6 shows the flux of through-going muons and the relative fraction of stopping upward muons as functions of zenith angle.

The χ^2 analysis described for the contained single-ring sample has been extended to include 15 additional angular bins for upward-going muons. For $\nu_\mu \leftrightarrow \nu_\tau$ oscillation hypothesis this combined analysis of 848 day sample provided the best-fit parameters: $\sin^2 2\theta = 1.0$ and $\Delta m^2 = 3.5 \times 10^{-3}$ eV^2, with $\chi^2/d.o.f. = 67.7/67$. The corresponding confidence contours are shown in Fig. 7 More details can be found in Ref. [18].

4. Solar Neutrinos

Solar neutrinos are observed in Super-Kamiokande via elastic neutrino-electron scattering in water:

$$\nu_e + e^- \longrightarrow \nu_e + e^- \qquad (4)$$

Due to kinematics of the reaction the electron follows the neutrino direction. Therefore the angle $\theta_{\rm Sun}$ between reconstructed electron direction and the current direction away from the Sun can be used to separate solar neutrino interactions from background events (see Fig. 8).

As a result of the analysis of 708 days of data $9530^{+167}_{-155}(\text{stat.})^{+266}_{-257}(\text{syst.})$ signal events above 6.5 MeV recoil electron energy were selected. From this number the total ^{8}B solar neutrino flux can be calculated to be $(2.44 \pm 0.04(\text{stat.}) \pm 0.07(\text{syst.})) \times 10^6/\text{cm}^2/\text{sec}$. It is significantly lower than expected from the BP98[20] Standard Solar Model (SSM). The ratio is $\frac{\text{Data}}{\text{SSM}_{\text{BP98}}} = 0.470^{+0.008}_{-0.007}(\text{stat.}) \pm 0.013(\text{syst.})$

The discrepancy between SSM and the flux measurement may be explained by oscillation of electron neutrinos $\nu_e \leftrightarrow \nu_x$ into another neutrino type, which interacts in the detector with much smaller cross section. In particular muon and tau neutrinos of a few MeV scatter on electrons only via NC and hence their detection rate is much smaller. Another possibility is an oscillation into a sterile neutrino.

If the Δm^2 between dominant components of ν_e and ν_x is very small ($< 10^{-9} eV^2$) then the flavor conversion occurs in "vacuum" when ν_e travels from the Sun to Earth. If Δm^2 is larger, then the MSW resonant enhancement causes a flavor transformation in the dense solar matter.

Super-Kamiokande allows to study the oscillation hypotheses in a more model-independent way than only comparing the measured fluxes with predictions. In particular any difference between day and night fluxes, unexpected seasonal flux variation or a modulation of electron energy spectrum would provide a more convincing proof of a new neutrino physics.

4.1. Day-night effect

If the MSW effect in the solar matter is responsible for a $\nu_e \rightarrow \nu_x$ transition, then the $\nu_x \rightarrow \nu_e$ process may occur in the Earth core, leading to a regeneration of the electron neutrinos and an increase of the signal during nights.

The measured day–night asymmetry defined as

$$\frac{\text{day} - \text{night}}{\text{day} + \text{night}} = -0.029 \pm 0.017(\text{stat.}) \pm 0.013(\text{syst.})$$

differs not significantly from zero.

A more sensitive search for the effect is presented in Fig. 9, which shows the neutrino flux above 6.5 MeV as a function of the zenith angle of the current Sun position. A small flavor mixing would result in an increase in flux when the neutrinos pass through the Earth core, i.e. the effect would only appear in the 'night 5' bin in figure 9. Larger flavor mixing predicts an enhancement throughout the night. Constraints on neutrino oscillation parameters from the lack of a significant day-night effect are published in [12].

4.2. Solar neutrino spectrum

Although the Super-Kamiokande measures the energy spectrum of recoil electrons, its shape directly reflects the shape of the spectrum of incoming neutrinos (c.f. reaction 4). Precision energy calibration have been done [11] with various sources, in particular using an electron linear accelerator providing a tunable energy ranging from 5 to 16 MeV. The uncertainty in the energy scale is estimated to be $\pm 0.8\%$, while the energy resolution is better than 2%.

The event rates are determined in 0.5 MeV energy bins using for each bin the distributions of θ_{Sun} and extracting a solar peak as in Fig. 8. Below 6.5 MeV a background due to radioactive impurities increases sharply with decreasing energy. A new Super Low Energy (SLE) analysis was designed to reject these backgrounds more efficiently. Currently, the SLE analysis threshold is at 5.5 MeV (c.f. Ref. [19]).

A convenient way to search for spectral distortions is to divide the observed spectrum by the energy spectrum of simulated electrons based on the SSM neutrino flux expectations (see Fig. 10). Thus the experimental energy resolution is taken into account.

The best fit to the spectrum shape is obtained for vacuum oscillation with $\sin^2 2\theta = 0.87$ and $\Delta m^2 = 4.3 \times 10^{-10}$ eV^2. Matter enhanced (MSW) neutrino oscillations would cause smaller modulation of the spectrum.

However the observed relative increase in the flux at the end of the spectrum can also be explained [21] by much higher than expected flux of "Hep" neutrinos resulting from the process:

$$^3\text{He} + p \longrightarrow {}^4\text{He} + e^+ + \nu_e.$$

According to the SSM Hep neutrinos contribution is very small but its flux is highly uncertain. Therefore a fit was done to the spectrum shape with relative contribution of Hep flux as a free parameter. As shown in Fig. 11 an increase in the Hep flux of a factor of about twenty with respect to the SSM is needed to fit the data.

Clearly more data are needed to solve the puzzle at the end of the spectrum. The uncertainty of the Hep flux does not affect lower energies. Therefore a large effort is now undertaken towards decreasing the threshold down to 5 or even 4.5 MeV.

4.3. Seasonal variation

Since the distance from Sun to Earth changes with a yearly cycle, vacuum oscillations can cause a seasonal modulation of the neutrino flux on top of the conventional $\frac{1}{r^2}$ flux dependence (indicated with a solid line in Fig. 12). Interestingly, it has been pointed out in Ref. [22] that also MSW oscillations can cause a seasonal flux modulation, if a significant ν_e regeneration occurs in the Earth, which obviously depends on how long the Sun is under horizon.

After less than three years of data taking, the statistical accuracy is insufficient to observe this effect. The data slightly favors the presence of seasonal variation above 11.5 MeV, but more data is needed to observe a significant effect.

5. Summary

Precise measurements of angular distributions of atmospheric neutrinos in the Super-Kamiokande detector provide a clear evidence for muon neutrino oscillations. The best interpretations of data is obtained for $\nu_\mu \leftrightarrow \nu_\tau$ flavor transformation with maximal mixing and a mass difference of 0.05 to 0.07 eV. The evidence comes from the sample of contained single ring events, but

is confirmed by 2-ring events as well as upward-going muon sample.

The data can also be explained by oscillations into sterile neutrinos. A difference between the $\nu_\mu \leftrightarrow \nu_\tau$ and $\nu_\mu \leftrightarrow \nu_s$ scenarios can be revealed in the rate and angular distributions of NC events

$$\nu_l + N \rightarrow \nu_l + \pi^0 + N', \quad (5)$$

which do not occur for ν_s while have the same cross-sections for ν_μ and ν_τ. The K2K experiment [23] gives a chance to improve our knowledge of pion production in water in order to reduce systematic errors.

A suppression of $\nu_\mu \leftrightarrow \nu_s$ due to matter effects expected for a small $\Delta m^2/E_\nu$ values also gives a chance for a resolution of the ν_τ and ν_s scenarios.

The solar neutrino puzzle has been complicated by a large uncertainty in the Hep neutrino flux, which underlines the necessity for still more precise measurements of the ^{8}B neutrino spectrum, especially at the lowest energies. No significant day-night effect has been observed. There is however a hint in a modulation of seasonal flux variation, but more statistics is needed.

6. Acknowledgements

The Super-Kamiokande experiment is supported by the Japanese Ministry of Education, Science, Sports and Culture and the United States Department of Energy. DK gratefully acknowledges the support of Polish Committee for Scientific Research by a grant number 2P03B05316. The author is thankful to organizers for the kind invitation and the hospitality extended to her at the workshop.

REFERENCES

1. M. Honda *et al.*, *Phys. Rev.* **D52** (1995) 4985, *Prog. Theor. Phys. Suppl.* **123** (1996) 483.
2. G. Barr *et al.*, *Phys. Rev.* **D39** (1989) 3532. V. Agrawal *et al. Phys. Rev.* **D53** (1996) 1313. hep-ph/9509423 T. K. Gaisser and T. Stanev, Proc. 24th Int. Cosmic Ray Conf. (Rome) Vol. 1 (1995) 694.
3. T. J. Haines *et al.*, *Phys. Rev. Lett.* **57** (1986) 1986;
   D. Casper *et al.*, *Phys. Rev. Lett.* **66** (1991) 2561;
   R. Becker-Szendy *et al.*, *Phys. Rev.* **D46** (1992) 3720.
4. K. S. Hirata *et al.*, *Phys. Lett.* **B205** (1988) 416;
   K. S. Hirata *et al.*, *Phys. Lett.* **B280** (1992) 146.
5. W. W. M. Allison *et al. Phys. Lett.* **B449** 137 (1999). hep-ex/9901024
6. Y. Fukuda *et al.*, *Phys. Lett.* **B335** (1994) 237.
7. Y. Fukuda *et al.*, *Phys. Lett.* **B433** (1998) 9, hep-ex/9803006;
   Y. Fukuda *et al.*, *Phys. Lett.* **B436** (1998) 33, hep-ex/9805006;
   Y. Fukuda *et al.*, *Phys. Rev. Lett.* **82** (1999) 2644, hep-ex/9812014.
8. Y. Fukuda *et al.*, *Phys. Rev. Lett.* **81** (1998) 1562, hep-ex/9807003
9. S.P. Mikheev and A.Y. Smirnov, *Nuovo Cim.*, **9C**, (1986) 17;
   L. Wolfenstein, *Phys. Rev.* **D17**, (1978) 2369.
10. Y. Fukuda *et al.*, *Phys. Rev. Lett.* **81** (1998) 1158, hep-ex/9805021 and refs herein.
11. Y. Fukuda *et al.*, *Phys. Rev. Lett.* **82** (1999) 2430, hep-ex/9812011;
    M. Nakahata *et al.*, *Nucl. Instr. Meth.* **A421** (1999) 113, hep-ex/9807027.
12. Y. Fukuda *et al.*, *Phys. Rev. Lett.* **82**, (1999) 1810, hep-ex/9812009
13. T. K. Gaisser, talk presented at *The 17th International Conference on Neutrino Physics and Astrophysics, NEUTRINO 96*, Helsinki, 1996, (hep-ph/9611301)
14. K. Scholberg for the Super-Kamioande Collaboration, talk presented at *8th International Workshop on Neutrino Telescopes*, Venice, Feb. 1999; hep-ex/9905016
15. M. D. Messier, PhD thesis, Boston University (1999).
16. P. Lipari, T. K. Gaisser and T. Stanev, *Phys. Rev.* **D 58**, (1998) 073003. hep-ph/9803440
17. T. Futagami *et al.*, submitted to *Phys. Rev. Lett.*. astro-ph/9901139
18. A. Habig for the Super-Kamiokande collaboration, Proceedings of DPF '99 (UCLA). hep-ex/9903047

19. M. B. Smy for the Super-Kamiokande collaboration, Proceedings of DPF '99 (UCLA). hep-ex/9903034
20. J. Bahcall, S. Basu, and M. Pinsonneault, *Phys. Lett. B.*, **433,** 1 (1998).
21. R. Escribano *et al.*, *Phys. Lett.* **B444**, (1998) 397, hep-ph/9805238
22. P. C. de Hollanda *et al.*, hep-ph/9903473
23. Y. Oyama for the K2K collaboration, talk at the YITP workshop on flavor physics, Kyoto (1998); hep-ex/9803014

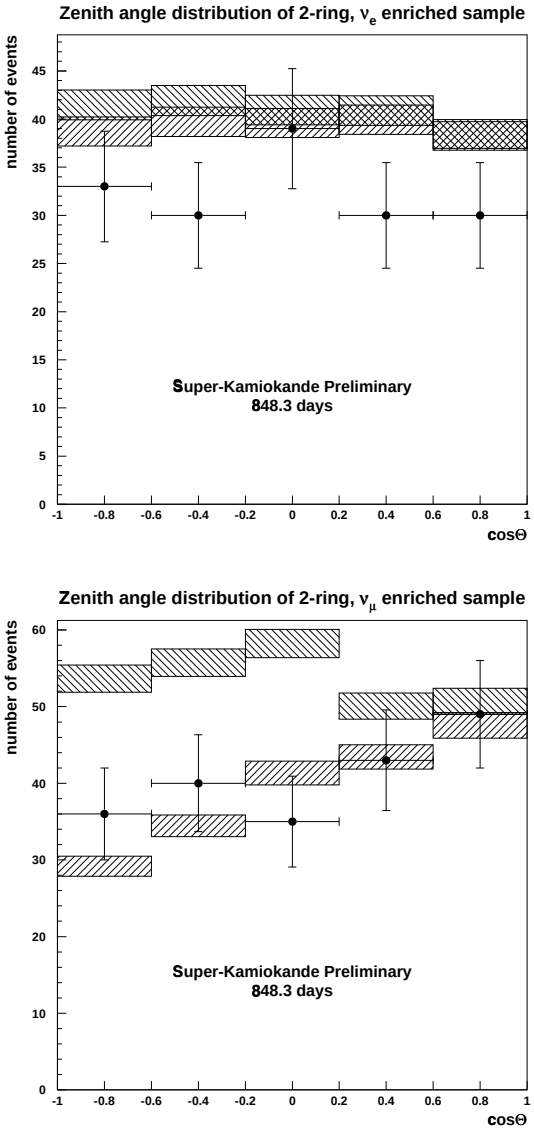

Figure 5. Zenith angle distributions for ν_e enriched (top) and ν_μ enriched (bottom) subsamples of 2-ring events. The left-hatched bars show the MC prediction for no oscillation and the right-hatched bars show the prediction for the oscillation parameters $\sin^2 2\theta = 1$ and $\Delta m^2 = 3.5 \times 10^{-3}$ eV^2.

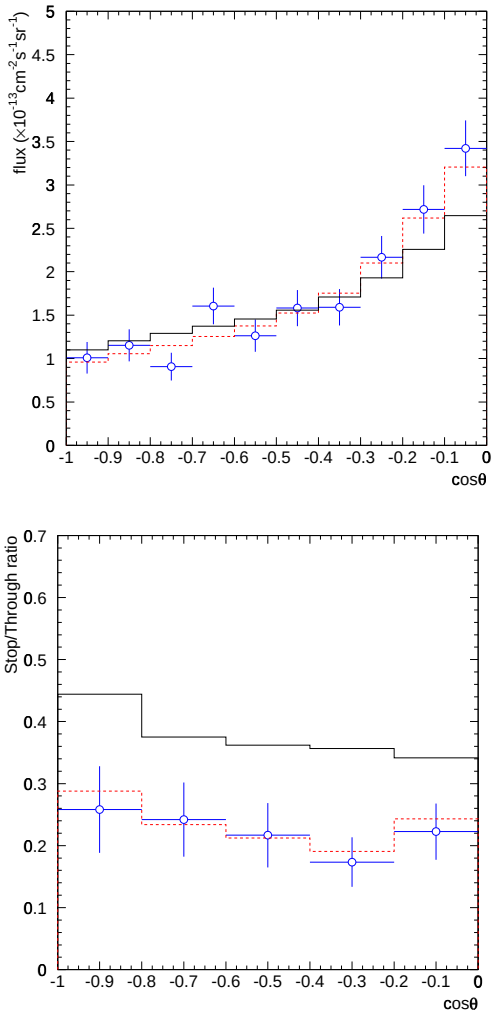

Figure 6. Top: Zenith angle distribution of through-going upward muons (537 day sample). Bottom: ratio of stopping to through-going muons as a function of $\cos\theta$. The circles represent the data, the solid lines show the no-oscillation flux predictions, and the dashed lines are for the best fit $\nu_\mu \leftrightarrow \nu_\tau$ oscillations.

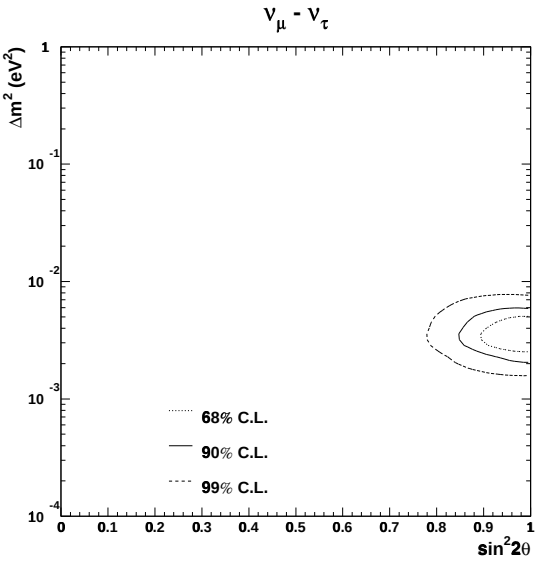

Figure 7. Allowed regions using combined information from FC, PC and upward-going muons.

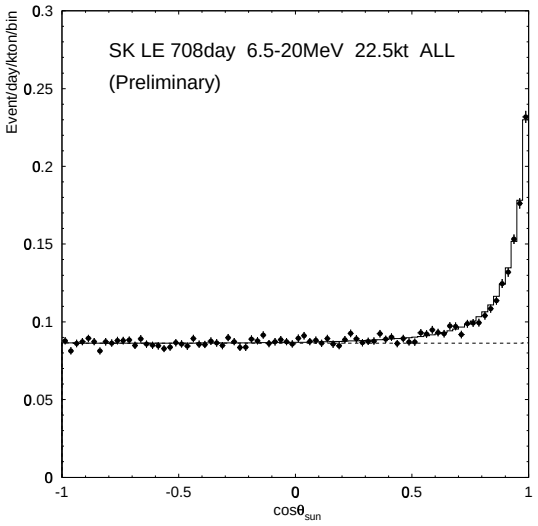

Figure 8. Angular distribution of electrons with respect to the direction of the Sun. The 'solar peak' at $\cos\theta_{\rm Sun} = 1$ above the background is used to measure the solar ^{8}B neutrino flux and spectrum.

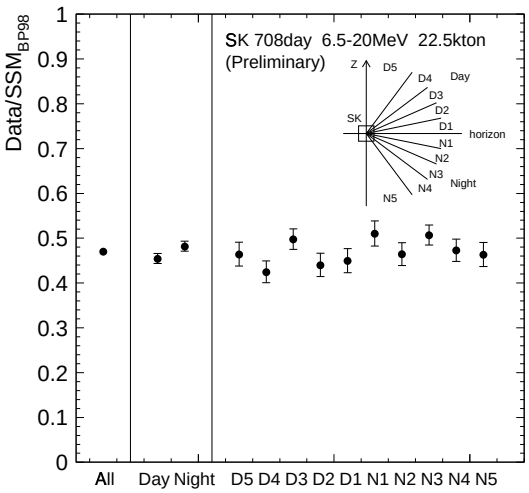

Figure 9. Neutrino flux as a function of the zenith angle of the Sun's position. The bins are defined in the figure.

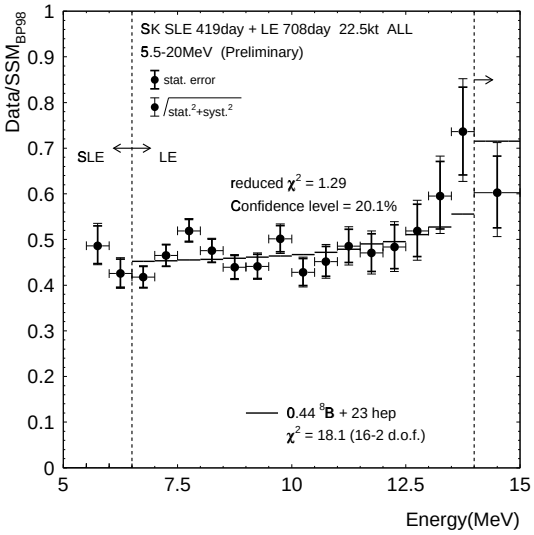

Figure 11. Best no oscillation fit without constraint on the ^{8}B or Hep flux normalization.

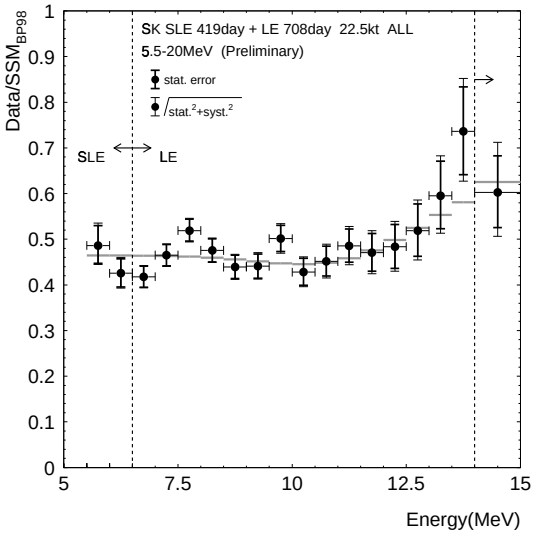

Figure 10. Electron spectrum normalized to the SSM expectations. Histogram shows the best fit to the spectrum shape (vacuum oscillation with $\sin^2 2\theta = 0.87$, $\Delta m^2 = 4.3 \times 10^{-10}$ eV^2).

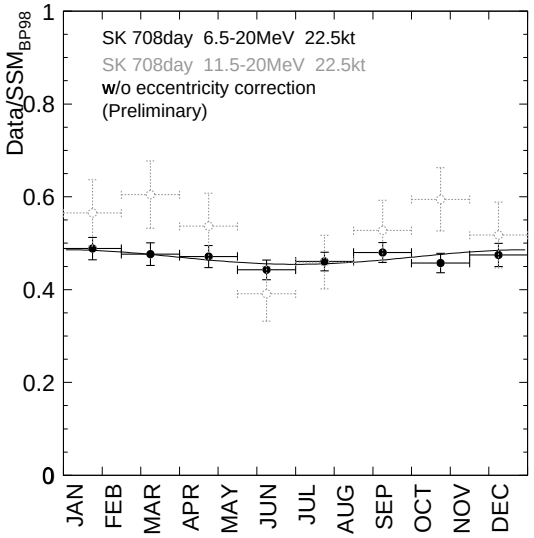

Figure 12. The seasonal variation for the flux above 6.5 MeV (black filled in circles) and 11.5 MeV (grey open circles). The black line accounts for the variation expected from the Earth orbit eccentricity.